IL NUOVO CIMENTO VOL. 28 A, N. 4 21 Agosto 1975

Jet Structure and Scaling in e^+e^- Annihilation.

R. BAIER, J. ENGELS and H. SATZ

Department of Theoretical Physics, University of Bielefeld - Bielefeld

K. SCHILLING

Physics Department, University of Wuppertal - Wuppertal

(ricevuto il 12 Febbraio 1975)

Summary. — An uncorrelated jet model, with randomly oriented jet axis and parameters as determined from high-energy hadronic interactions, is applied to e^+e^- annihilation. The resulting features (multiplicities, spectra, correlations, branching ratios) are calculated both at finite c.m.s. energies ($(3 \div 5)$ GeV) and asymptotically, in order to study the approach to asymptotic behaviour expected for quark, parton and similar models. It is shown that such descriptions, where the jet structure is the same as in hadron-hadron interactions, lead for kinematic reasons to very late scaling of the normalized inclusive hadron distribution. Our results are compared with cluster models for e^+e^- annihilation and with data.

1. – Introduction.

Two aspects of e^+e^- annihilation make this process a rather unique tool for the investigation of hadron production: it is, within the region of validity of the one-photon approximation, the only experimentally feasible way to prepare a high-mass hadronic system of spin one, and when combined with information from deep inelastic e-p scattering, it allows us to study photon-hadron interactions with the photon mass varying continuously from large spacelike to large timelike values. The first aspect permits us to investigate hadron dynamics without the complications of a highly anisotropic initial state, which are always present in hadron-hadron collisions, and the latter provides us in

the timelike region of the photon mass with constraints from experiments in the spacelike region (*e.g.* Bjorken scaling) and *vice versa*.

This challenging situation has led to much theoretical speculation [1], restrained now, however, by the increasing flow of data on high-energy e^+e^- annihilation [2]. These experiments provide information on two main and *a priori* independent features of hadron production via a single heavy photon of mass $M = \sqrt{q^2}$: the q^2-dependence of the total cross-section $\sigma_{tot}(e^+e^- \to \text{hadrons})$, and the distribution of this cross-section over the allowed inelastic channels, expressed *e.g.* in the form of normalized single-particle spectra

$$\frac{2p_0}{\sigma_{tot}} \frac{d^3\sigma}{d^3p}$$

with $p_0 = \sqrt{p^2 + m^2}$ denoting the c.m.s. energy of the observed secondary, m its mass. While some models (in particular those postulating hadrons made up of pointlike constituents) discuss both features simultaneously, we shall here restrict ourselves to a study of the relative structure of hadron production channels, independently of the q^2-behaviour of σ_{tot}. This gives us the advantage of being able to deal with many-particle aspects in a fashion as general as possible; we must pay for it by leaving open the question of connecting our results for timelike photons with those for the spacelike photons of deep inelastic e-p interactions.

From a phenomenological point of view, the great variety of theoretical descriptions proposed for multiparticle production in e^+e^- annihilation can be divided into two classes [3,4]: Most parton [5], quark [6] and similar constituent models [1] provide for the normalized distribution in the c.m.s. energy p_0 of the secondary, as function of the virtual-photon mass $\sqrt{q^2}$

$$F(q^2, p_0) = \frac{1}{\sigma_{tot}} \int d^2\Omega \, 2p_0 \frac{d^3\sigma}{d^3p} \tag{1.1}$$

---

[1] Cf. *e.g.* J. D. BJORKEN: in *Proceedings of the VI International Symposium on Electron and Photon Interactions at High Energies, Bonn, 1973* (Amsterdam, 1974); C. H. LLEWELLYN-SMITH: *Erice Lectures, 1974*, to be published; J. ELLIS: invited talk held at the *XVII International Conference on High-Energy Physics* (London, 1974), Rutherford Laboratory (1974).

[2] B. RICHTER: *Proceedings of the XVII International Conference on High-Energy Physics* (London, 1974), Rutherford Laboratory (1974).

[3] J. D. BJORKEN and S. BRODSKY: *Phys. Rev. D*, **1**, 1416 (1970).

[4] I. ANDRIĆ, I. DADIĆ and H. SATZ: Bielefeld preprint Bi-74/20, *Nucl. Phys.* (in press).

[5] S. D. DRELL, D. J. LEVY and T. M. YAN: *Phys. Rev. D*, **1**, 1617 (1970).

[6] R. GATTO and G. PREPARATA: *Nucl. Phys.*, **67 B**, 362 (1973).

[7] N. CABIBBO, G. PARISI and M. TESTA: *Lett. Nuovo Cimento*, **4**, 35 (1970).

a « scaling » form when $q^2 \to \infty$

$$F_0(q^2, p_0) = \varphi_0(2p_0/\sqrt{q^2}) . \tag{1.2}$$

In eq. (1.1) Ω denotes the angular orientation of the observed secondary in the overall c.m.s. The result eq. (1.2) is most easily visualized in the form of a photon coupling to a constituent-anticonstituent pair, with the latter then radiating secondaries. It should be kept in mind, however, that such a jet picture [7] with randomly oriented axis is (as shown in ref. [8]) not the only way to realize eq. (1.2); also, it is certainly possible (*e.g.* by final-state interaction) to construct constituent-anticonstituent models which provide neither jet structure nor scaling [9]. In the second group of models the single-particle spectra contain a dimensional parameter R: asymptotically

$$F_\nu(q^2, p_0) \simeq g_\nu(q^2)\varphi_\nu\left(\frac{R^\nu 2p_0}{(q^2)^{(1-\nu)/2}}\right) \tag{1.3}$$

with $0 < \nu \leqslant 1$; such a behaviour is generally given by cluster-type descriptions, as the statistical [8,10], statistical bootstrap [8] and hydrodynamical [11] model. Here, however, we should remember that one can also construct jet models leading to eq. (1.3), because transverse-momentum (p_T) bounds and scaling are in general independent properties of production processes [*]. While eq. (1.3) for $\nu = 0$ gives us back the scaling form eq. (1.2) it provides for $\nu = 1$ a special case realized in the statistical bootstrap model

$$F_1(q^2, p_0) \simeq g_1(q^2)\varphi_1(p_0) , \tag{1.4}$$

and which we shall therefore call a fireball distribution. Scaling and fireball spectra are thus in a sense opposite possible extremes for single-particle distributions of hadrons emitted in e^+e^- annihilation at high energies. In order to investigate the consequence of these two extremes, it seems to us best to study simple prototype models of each type. In ref. [8,12] we have carried out the first

---

[8] J. ENGELS, H. SATZ and K. SCHILLING: *Nuovo Cimento*, **17** A, 535 (1973).
[9] I. MONTVAY and N. CABIBBO: private communication.
[10] MENG TA CHUNG: Freie Universität Berlin, preprint FUB HEP Jan 74/2; W. S. LAM and E. SUHONEN: *Phys. Lett.*, **50** B, 453 (1974).
[11] E. V. SHURYAK: *Phys. Lett.*, **34** B, 509 (1971); E. L. FEINBERG: *Phys. Rep. C*, **5**, 237 (1972); F. COOPER, G. FRY and E. SCHONBERG: *Phys. Rev. Lett.*, **32**, 862 (1974), and references quoted therein.
[*] Note here that dual-resonance models do not provide a criterion to choose between jet and cluster description, cf. ref. [4].
[12] J. ENGELS, H. SATZ and K. SCHILLING: *Phys. Lett.*, **49** B, 171 (1974).

step of this program by calculating the main predictions resulting from the statistical bootstrap model for e^+e^- annihilation, both at finite energies and asymptotically. This description (for one type of secondaries) contains essentially one open parameter, the ultimate temperature of hadronic matter, which we fixed by using high-energy hadron-hadron data, specifically, the p_T-distribution of the secondaries.

The aim of the present paper will be to complete this program by calculating the analogous predictions for a general model of the « scaling » type. We consider for this purpose as most suitable form that given by an uncorrelated jet model ([13]) with arbitrary jet axis; as in the other extreme, the statistical bootstrap model, we shall fix the open parameters (here two, as we shall see) by their values in hadron-hadron interactions. Again we shall calculate all predictions both at finite energies, particularly in the region presently accessible to experimenters, and asymptotically.

The onset of scaling is here—as in any model of scaling type—of particular interest: for what photon mass $\sqrt{q^2}$, at a given secondary energy p_0, will the asymptotic form really be attained? This question, apparently never studied anywhere in quantitative detail, will form a main part of our work and leads to quite striking results (*): we shall show explicitly that for jets of « hadronic dimensions » scaling at present energies is in fact kinematically forbidden for all $x = 2p_0/\sqrt{q^2} < 1$.

We should stress here the importance of the hypothesis of « hadronic dimensions »: the main features of the scaling and fireball ([8]) type are of rather general nature, but the point of transition between low-energy and asymptotic behaviour is strongly dependent on the actual value of the parameters.

Let us furthermore underline again that all results will be independent of the behaviour of $\sigma_{tot}(e^+e^- \to \text{hadrons})$; we shall only consider normalized distributions of the type eq. (1.1), so that any q^2-dependence of the photon-hadron (or photon-parton, photon-quark) coupling will drop out.

The remainder of the paper is organized as follows. In Sect. **2** we shall present the uncorrelated jet model for e^+e^- annihilation, discuss the meaning of the parameters involved, and calculate the asymptotic behaviour of the model, particularly for the multiplicity, spectra, integrated correlation functions and branching ratios. In Sect. **3** we shall calculate the predictions for these quantities at present accelerator energies and study the approach to scaling.

([13]) L. VAN HOVE: *Rev. Mod. Phys.*, **36**, 655 (1964); A. KRZYWICKI: *Nuovo Cimento*, **32**, 1067 (1964).

(*) It should be noted here that by more qualitative arguments relating inclusive processes in pp scattering with those in e^+e^- annihilation GATTO and PREPARATA ([14]) came to similar conclusions.

([14]) R. GATTO and G. PREPARATA: *Phys. Lett.*, **50** B, 479 (1974).

2. – The jet model and its asymptotic behaviour.

The fully exclusive decay distribution of a virtual photon (we shall always assume that the photon decay is independent of its polarization) into N secondaries of momentum p_i, for simplicity chargeless pions, is in our model given by

$$\Gamma_N \sim \frac{\varkappa^N}{N!} \prod_{i=1}^{N} \frac{\mathrm{d}^3 p_i}{2p_{i0}} \delta^{(4)}\Big(\sum_{i=1}^{N} p_i - q\Big) \int \mathrm{d}^2\hat{e} \prod_{i=1}^{N} \exp\left[-\lambda |\boldsymbol{p}_i \times \hat{e}|\right] . \tag{2.1}$$

$\hat{e}$ is a unit vector specifying the jet axis of each event. According to the assumption made above, this axis is randomly oriented. In terms of the transversely cut-off phase-space volume

$$\Omega(\hat{e}, q) = \sum_{N=2}^{\infty} \frac{\varkappa^N}{N!} \int \prod_{i=1}^{N} \frac{\mathrm{d}^3 p_i}{2p_{i0}} \exp\left[-\lambda |\boldsymbol{p}_i \times \hat{e}|\right] \delta^{(4)}\Big(\sum_{i=1}^{N} p_i - q\Big) , \tag{2.2}$$

we then have for the normalized inclusive single-particle spectrum in the photon rest system

$$\frac{2p_0}{\sigma_{\mathrm{tot}}} \frac{\mathrm{d}^3\sigma}{\mathrm{d}^3 p} = \left\{ \int \mathrm{d}^2\hat{e}\, \varkappa \exp\left[-\lambda |\boldsymbol{p} \times \hat{e}|\right] \Omega(\hat{e}, q - p) \right\} \Big/ \int \mathrm{d}^2\hat{e}\, \Omega(\hat{e}, q) \equiv \tilde{F}(q^2, \boldsymbol{p}) , \tag{2.3}$$

which is connected to the secondary energy distribution

$$\frac{1}{\sigma_{\mathrm{tot}}} \frac{\mathrm{d}\sigma}{\mathrm{d}p_0} = 2\pi p \tilde{F}(q^2, |\boldsymbol{p}|) = \frac{2}{\sqrt{q^2}} \frac{1}{\sigma_{\mathrm{tot}}} \frac{\mathrm{d}\sigma}{\mathrm{d}x} \tag{2.4}$$

with $x = 2p_0/\sqrt{q^2}$. In this model the sum rules

$$\frac{1}{\sigma_{\mathrm{tot}}} \int \mathrm{d}x \frac{\mathrm{d}\sigma}{\mathrm{d}x} = \bar{N} , \tag{2.5}$$

$$\frac{1}{\sigma_{\mathrm{tot}}} \int \mathrm{d}x\, x \frac{\mathrm{d}\sigma}{\mathrm{d}x} = 2 , \tag{2.6}$$

are automatically satisfied.

The physical significance of the two parameters $\varkappa$ and λ is quite evident: λ^{-1} determines the jet width and $\varkappa$ essentially characterizes the multiplicity distribution, an increase in $\varkappa$ giving a higher weight to larger particle numbers.

The values of these parameters will be fixed from the average particle number $\bar{N}$ and the transverse-momentum distribution in high-energy hadron-hadron collisions by using asymptotic expressions of the uncorrelated jet model

(with the jet axis now fixed to the hadron beam direction)

$$\bar{N} \xrightarrow[q^2\to\infty]{} \tilde{\varkappa} \ln q^2 , \qquad \tilde{\varkappa} = \frac{\pi\varkappa}{\lambda^2} \tag{2.7}$$

and

$$2p_0 \frac{\mathrm{d}^3\sigma}{\mathrm{d}^3p}\bigg|_{p_L=0, p_T \text{ small}} \sim \exp\left[-\lambda|p_T|\right] . \tag{2.8}$$

From 90° pion spectra at the ISR one has $\lambda = 6.2\ (\mathrm{GeV})^{-1}$ ([15]). Moreover, this value appears universally valid for the various particle yields when plotted in the variable $\mu_T^i = \sqrt{p_T^2 + m_i^2}$. The energy dependence of the average charged multiplicities measured up to ISR energies is compatible with an asymptotic logarithmic behaviour and suggests $\tilde{\varkappa} = \pi\varkappa/\lambda^2 \approx 3$ ([16]). Being well aware that the precise values for λ and $\varkappa$ depend on the details of the fitting ([17]), we nevertheless consider these numbers as characteristic for hadronic dimensions.

With λ and $\varkappa$ thus determined from pp data, we now come back to e^+e^- annihilation in order to discuss the asymptotic expansions for the most relevant inclusive quantities predicted by the jet model. This will give us some feeling how fast an approach to asymptotia can be expected.

The evaluation of the asymptotic expansions was performed by the methods of ref. ([18]) and is described in some detail in the Appendix.

The deviations from the leading behaviour for $\bar{N}(q^2)$ and the integrated correlation $f_2 = \overline{N(N-1)} - \bar{N}^2$ can be written in the form of a series in $(\ln q^2)^{-1}$

$$\bar{N}(q^2) = \tilde{\varkappa}\left(\ln\frac{q^2}{4m^2}\right) \cdot \left[1 + \frac{c_1}{\ln(q^2/4m^2)} + \frac{c_2}{(\ln(q^2/4m^2))^2} + \frac{c_3}{(\ln(q^2/4m^2))^3} + \ldots\right], \tag{2.9}$$

$$f_2(q^2) = d\left[1 + \frac{d_1}{\ln(q^2/4m^2)} + \frac{d_2}{(\ln(q^2/4m^2))^2} + \ldots\right] . \tag{2.10}$$

With $\varkappa = 36\ (\mathrm{GeV})^{-2}$ and $\lambda = 6.2\ (\mathrm{GeV})^{-1}$, the actual values of the constants

---

([15]) See *e.g.* B. ALPER, H. BØGGILD, P. BOOTH, F. BULOS, L. J. CARROLL, G. JARLSKOG, L. JÖNSSON, A. KLOVNING, L. LEISTAM, E. LILLETHUN, G. LYNCH, S. ØLGAARD-NIELSEN, M. PRENTICE, D. QUARRIE and J. M. WEISS: *Phys. Lett.*, **47** B, 75 (1973).

([16]) E. L. BERGER: *Erice Lectures, 1973*, to be published.

([17]) See *e.g.* M. ANTINUCCI, A. BERTIN, P. CAPILUPPI, M. D'AGOSTINO-BRUNO, A. M. ROSSI, G. VANNINI, G. GIACOMELLI and A. BUSSIÉRE: *Lett. Nuovo Cimento*, **6**, 121 (1973).

([18]) A. BASSETTO, M. TOLLER and L. SERTORIO: *Nucl. Phys.*, **34** B, 1 (1971).

are (*)

$$(2.11)\qquad \begin{cases} \tilde{\varkappa} = 2.942\,, & c_1 = -3.55\,, \quad c_2 = 0.62\,, \quad c_3 = 3.48\,, \\ d = -6.05\,, & d_1 = 0.27\,, \quad d_2 = 1.15\,. \end{cases}$$

Obviously, the expansions eqs. (2.9) and (2.10) converge very slowly and the size of the coefficients indicates that these expressions provide meaningful approximations only at energies $\sqrt{q^2} \gtrsim (15 \div 20)$ GeV.

To complete the discussion on the multiplicity distribution, we quote the leading energy behaviour of the normalized N-particle cross-section predicted by the jet model [19] (for the interesting case of $N \ll \ln(q^2/4m^2)$)

$$(2.12)\qquad R_N(q^2) \equiv \frac{\sigma_N(q^2)}{\sigma_{\text{tot}}(q^2)} \simeq (q^2)^{-\tilde{\varkappa}} \frac{[\tilde{\varkappa} \ln(q^2/4m^2)]^{N-1}}{(N-1)!} \simeq \frac{\bar{N}^{N-1}}{(N-1)!} \exp[-\bar{N}],$$

which decreases essentially like $\exp[-\bar{N}(q^2)]$ with increasing energy.

The asymptotic behaviour of the inclusive x-distribution, $(1/\sigma_{\text{tot}})(\mathrm{d}\sigma/\mathrm{d}x)$, can be discussed from eqs. (2.3) and (2.4): first, we note that, for a given $\hat{e}$, $\Omega(\hat{e}, q-p)$ is a function of $p_T = |\boldsymbol{p} \times \hat{e}|$ and the longitudinal missing mass

$$(2.13)\qquad M_L = \left((\sqrt{q^2} - p_0)^2 - (\hat{e}\boldsymbol{p})^2\right)^{\frac{1}{2}} = \sqrt{q^2}\left(1 - x + \frac{m^2 + p_T^2}{q^2}\right)^{\frac{1}{2}}$$

with the asymptotic behaviour

$$(2.14)\qquad \Omega(\hat{e}, q-p) \underset{p_T \text{ small};\, M_L, \sqrt{q^2} \text{ large}}{\simeq} \frac{M_L^{2\tilde{\varkappa}-2}}{\ln M_L}\left(1 + O(\ln^{-1} M_L)\right).$$

For $1 - x \gg (m^2 + p_T^2)/q^2$ and large q^2, this amounts to scaling of

$$(2.15)\qquad \frac{\Omega(\hat{e}, q-p)}{\int \mathrm{d}^2\hat{e}'\, \Omega(\hat{e}', q)} \simeq (1-x)^{\tilde{\varkappa}-1}$$

in the photon rest system.

The remaining step is the summation over the direction $\hat{e}$, according to eqs. (2.3) and (2.4):

$$(2.16)\qquad \frac{1}{\sigma_{\text{tot}}} \frac{\mathrm{d}\sigma}{\mathrm{d}x} \approx 2\tilde{\varkappa} \frac{(1-x)^{\tilde{\varkappa}-1}}{(x^2 - 4m^2/q^2)^{\frac{1}{2}}} r^2 \int_0^{\pi/2} \mathrm{d}\theta \sin\theta \exp[-r \sin\theta]$$

(*) These values for λ and $\varkappa$ are used in all numerical calculations presented in this paper.

(19) See *e.g.* E. H. DE GROOT: *Nucl. Phys.*, **48** B, 295 (1972).

with

$$r = \frac{\lambda}{2}\sqrt{q^2}\left(x^2 - \frac{4m^2}{q^2}\right)^{\frac{1}{2}}.$$

If r is large (but x not too close to 1!), this leads to the scaling limit (*)

$$\frac{1}{\sigma_{\text{tot}}}\frac{\mathrm{d}\sigma}{\mathrm{d}x} \simeq \frac{2\tilde{\varkappa}}{x}(1-x)^{\tilde{\varkappa}-1} \approx \frac{6}{x}(1-x)^2 . \tag{2.17}$$

The approach to scaling is discussed in detail in the Appendix.

An estimate of the actual numerical behaviour of $(1/\sigma_{\text{tot}})(\mathrm{d}\sigma/\mathrm{d}x)$ can be made from the asymptotic expansion, eq. (A.20): as a result, we would expect the deviations from the scaling curve, eq. (2.17), at 20 GeV to be of the order of 10 % or less only in the region $0.1 \leqslant x \leqslant 0.45$, with the minimal deviation around $x \simeq 0.2$.

Summarizing, within the jet model we expect scaling for $(1/\sigma_{\text{tot}})(\mathrm{d}\sigma/\mathrm{d}x)$ first to occur for x values away from one and zero. The reason for a slow approach to scaling in the vicinity of $x = 1$ is that here the unobserved system has a low missing mass (cf. eq. (2.13)) and hence $\Omega(\hat{e}, q-p)$ is not asymptotic.

On the other hand, near $x = 0$ (but above threshold $x_{\text{th}} = 2m/\sqrt{q^2}$) the transverse momentum of the observed secondary has to be taken into account and induces additional scaling violations of the order $O(1/\lambda^2 x^2 q^2)$ ([21]).

Here it must be emphasized again, however, that these methods yield reasonable approximations (with $\varkappa$ and λ as given) only for $\sqrt{q^2} \leqslant (15 \div 20)$ GeV/c. At lower energies, exclusive channels with nonasymptotic behaviour provide significant contributions to inclusive quantities; here we are still in the transition region between three-dimensional threshold behaviour and the one-dimensional asymptotic regime ([22]). Thus an explicit calculation of all exclusive terms is a much more suitable approach. In the next Section we shall therefore investigate the finite-energy behaviour of the jet model through numerical evaluation of the longitudinal phase-space integrals.

(*) It should be noted that the jet model with hadronic jet dimensions yields a quadratic dependence in $1-x$ in accord with the Drell-Yan-West relation from e-p scattering ([20]). We thank M. CHAICHIAN for pointing this out.

([20]) S. D. DRELL and T. M. YAN: *Phys. Rev. Lett.*, **24**, 181 (1970); G. WEST: *Phys. Rev. Lett.*, **24**, 1206 (1970).

([21]) T. F. WALSH and P. ZERWAS: *Nucl. Phys.*, **77** B, 494 (1974); J. ELLIS: invited talk held at the *XVII International Conference on High-Energy Physics* (London, 1974), Rutherford Laboratory (1974).

([22]) E. L. BERGER and A. KRZYWICKI: *Phys. Lett.*, **36** B, 380 (1971); H. SATZ: CERN Th-1905 (1974), to be published in *Proceedings of the IX Balaton Symposium, Balatonfüred, Hungary, June 1974.*

3. – Finite-energy behaviour and the approach to scaling.

To study finite-energy behaviour and the approach to scaling in our model and to obtain distributions which can be compared to data, we have carried out numerical calculations at $\sqrt{s} = \sqrt{q^2} = 1, 3, 3.8, 4.8, 20$ GeV, using a Monte Carlo program with appropriate importance sampling ([23]).

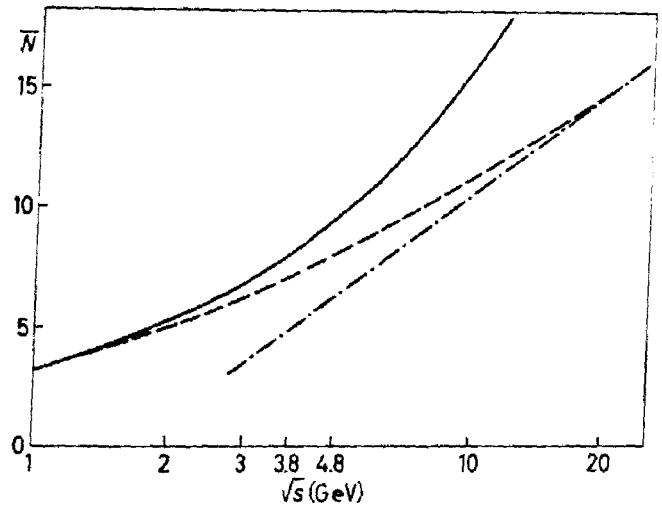

Fig. 1. – The mean particle multiplicity $\bar{N}$ predicted by the jet model for $\varkappa = 36$ (GeV)$^{-2}$ and $\lambda = 6.2$ (GeV)$^{-1}$ (broken line), by phase space for $\varkappa = 36$ (GeV)$^{-2}$ (solid line) and the asymptotic form $\bar{N} = \varkappa \ln s + c$ of the jet model (dash-dotted line).

The calculations of $\bar{N}$ and f_2 confirm the expectations expressed in the previous Section: with the given hadronic parameters the model reaches asymptotia not before $\sqrt{s} \approx 20$ GeV. This is evident in Fig. 1, which shows how the jet model result for $\bar{N}$, starting from pure phase space, approaches its asymp-

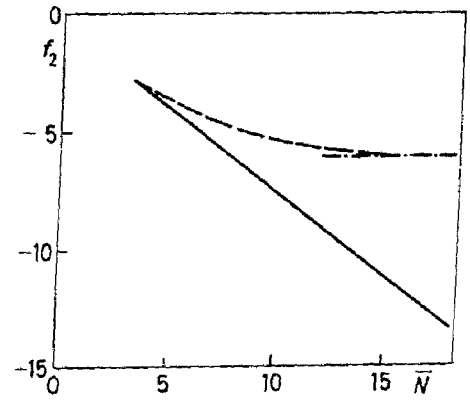

Fig. 2. – The correlation function f_2 predicted by the jet model (broken line), by phase space (solid line) and the asymptotic form $f_2 = \text{const}$ of the jet model (dash-dotted line).

([23]) W. KITTEL, L. VAN HOVE and W. WOJCIK: *Computer Phys. Comm.*, **1**, 425 (1970).

totic form $\bar{N} = \tilde{\varkappa} \ln s + c$; here the phase-space curve is obtained from eq. (2.2) with $\varkappa = 36\ (\mathrm{GeV})^{-2}$ and $\lambda = 0$ ([24]). In Fig. 2, the integrated correlation function f_2 behaves in a similar way. In particular we note that the jet model predicts a constant asymptotic value for f_2, whereas cluster models lead to constant $f_2/\bar{N}$ ([10,25]).

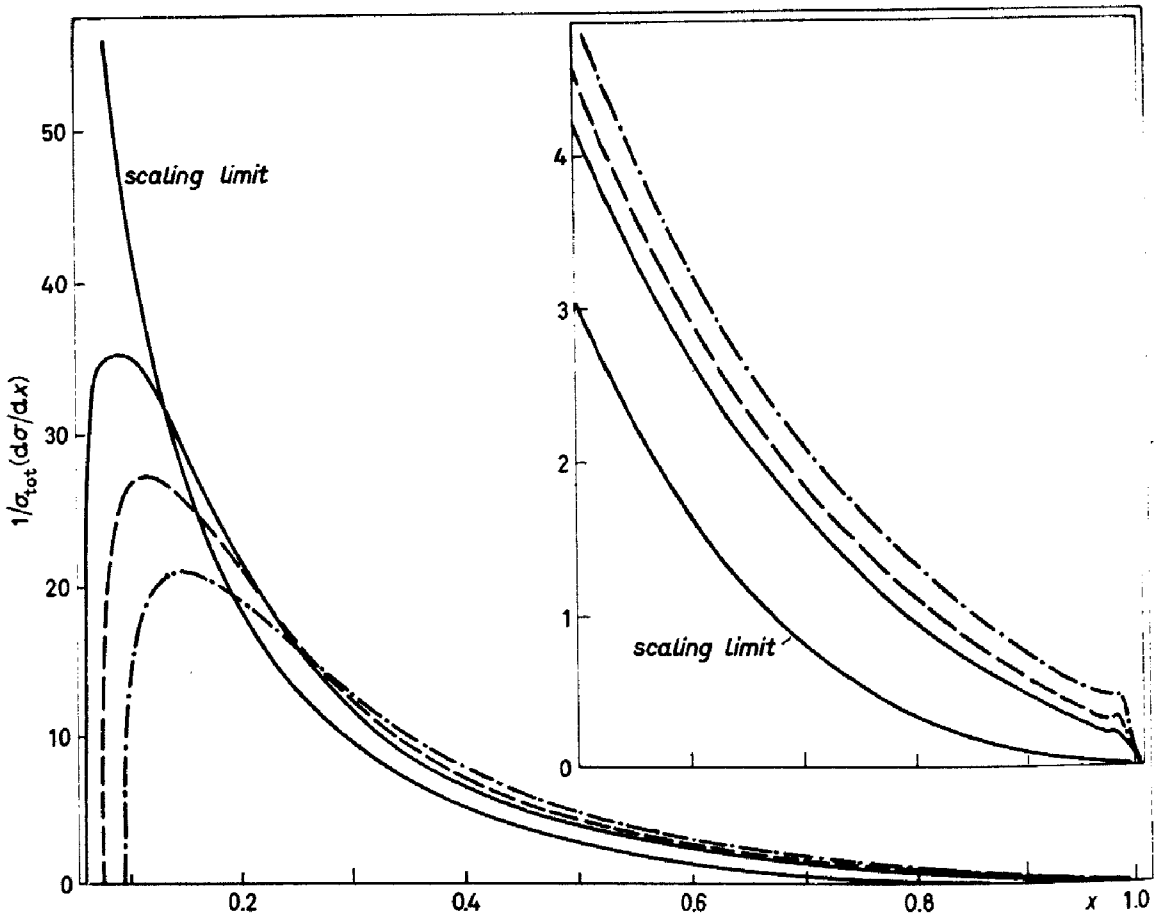

Fig. 3. – The inclusive one-particle spectra $(1/\sigma_{tot})(d\sigma/dx)$, $x = 2E_\pi/\sqrt{s}$ in the jet model at $\sqrt{s} = 3$ (dash-dotted line), 3.8 (broken line), 4.8 GeV (solid line) and the scaling curve eq. (2.17) (solid line).

The inclusive one-particle spectra $(1/\sigma_{tot})(d\sigma/dx)$ at 3, 3.8 and 4.8 GeV are compared with their scaling limit, eq. (2.17), in Fig. 3. Evidently, there is no sign of scaling for the normalized x-distribution at present SPEAR energies. If one did not know, however, the scaling limit, one might misinterpret the slow energy variation for $3\ \mathrm{GeV} \leqslant \sqrt{s} \leqslant 4.8\ \mathrm{GeV}$ and $x \geqslant 0.6$ as early scaling. We have therefore displayed this part of the distribution with an enlarged scale. We observe that the small shoulders near $x = 1$ are due to the low-multiplicity con-

([24]) We have used a computer program developed by K. KAJANTIE and V. KARIMÄKI: *Computer Phys. Comm.*, **2**, 207 (1971).

([25]) J. ENGELS, K. FABRICIUS and K. SCHILLING: *Nuovo Cimento*, **23** A, 581 (1974); *Phys. Lett.*, **53** B, 65 (1974).

tributions ($N = 3, 4, 5$). The dramatic increase of the small-x region with energy is, of course, connected to the rise in $\bar{N}$, as follows from the sum rule eq. (2.5).

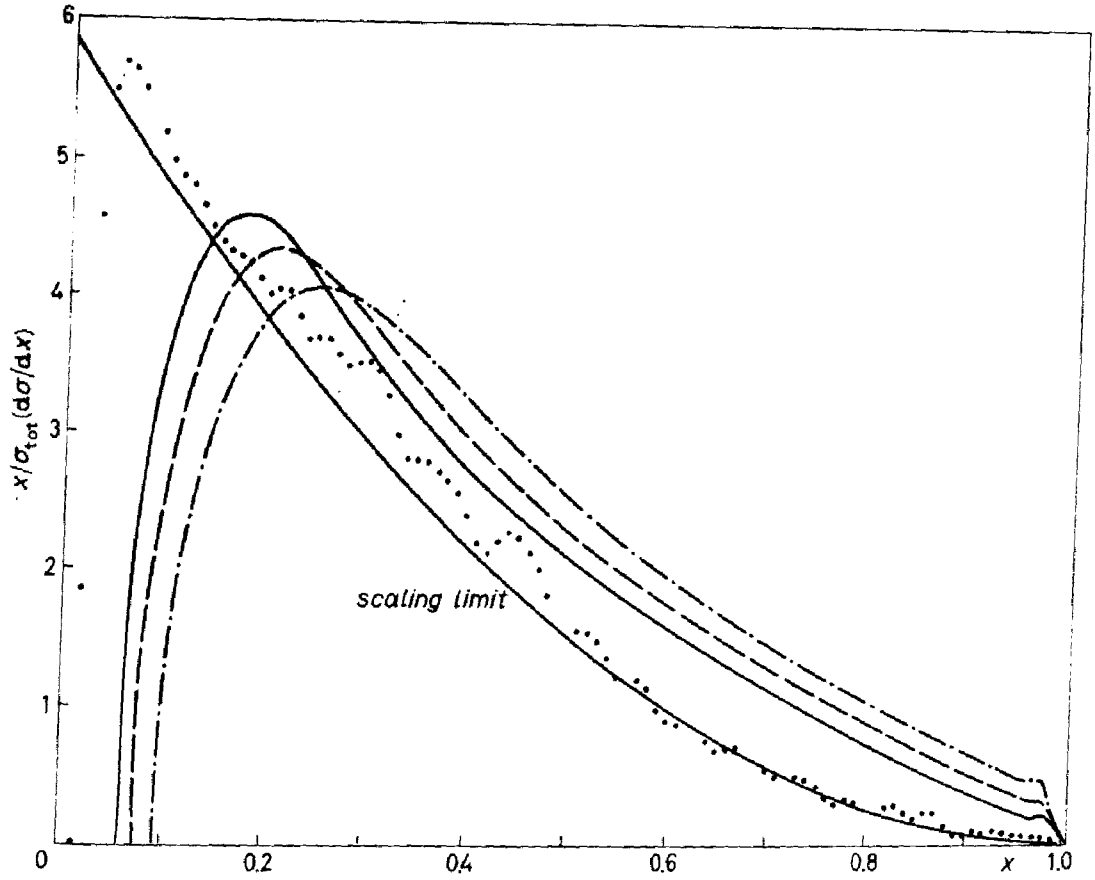

Fig. 4. – The inclusive one-particle spectra multiplied by x; the points are the result of a 20 GeV Monte Carlo calculation, the notation for the other curves is as in Fig. 3.

To discuss the relation of the finite-energy curves to the scaling limit, it is convenient to plot $(x/\sigma_{tot})(d\sigma/dx)$, which obeys eq. (2.6). Since, by phase space, the finite-energy curves for small x have to be below the scaling limit, they must be above the scaling curve at larger x in order to compensate for the « missing area » in the sum rule, eq. (2.6). This is visualized in Fig. 4, which also contains the results of a 20 GeV Monte Carlo calculation that has been performed with less statistics because of limited computer time. Within the statistical errors, this computation confirms the estimate resulting from the asymptotic expansion, eq. (A.20), according to which the deviations from the scaling curve are of the order of 10 % or less at $\sqrt{q^2} = 20$ GeV and $0.1 \leqslant x \leqslant 0.45$. Moreover, the Monte Carlo calculation suggests that this holds true up to $x = 0.8$.

At 4.8 GeV we have made a comparison of the normalized invariant single-particle distributions following from the jet model, the statistical bootstrap model (full bootstrap ([8,12]) with $T_0 = 160$ MeV and pions only), and simply invariant phase space as shown in Fig. 5: the jet model predicts a shape that

clearly deviates from phase space and results in a particle yield which is about one order of magnitude above phase space for large E_π, thus revealing the dynamics of jet formation. It is certainly more difficult to discriminate at this energy between a fireball model and phase space.

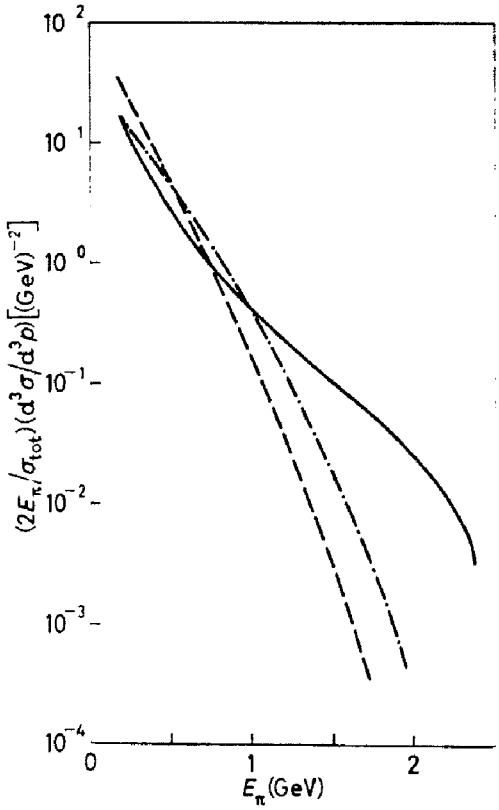

Fig. 5. – The normalized invariant one-particle cross-sections at 4.8 GeV following from the jet model (solid line), phase space (dash-dotted line) and the statistical full bootstrap model ($T_0 = 160$ MeV, pions only; broken line).

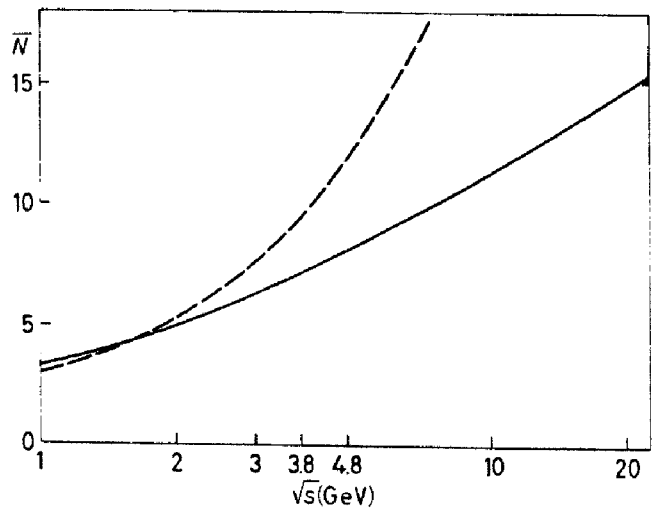

Fig. 6. – The mean particle multiplicity $\overline{N}$ for the jet model (solid line) and the statistical full bootstrap model ($T_0 = 160$ MeV, pions only; broken line).

Figures 6 and 7 show the different energy behaviour of $\bar{N}$ and f_2 predicted by the jet model and the statistical bootstrap model. Since the $\bar{N}$ predictions differ significantly already in the region $(5 \div 10)$ GeV, fairly good multiplicity data could provide a critical test.

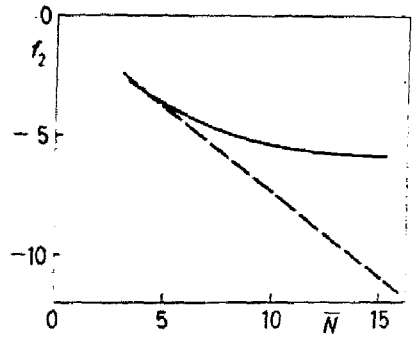

Fig. 7. – The correlation function f_2; same notation as in Fig. 6.

We want to remind the reader, however, that our present calculations are intended to show only the qualitative features. For a quantitative comparison with data one certainly has to refine the jet model presented here (*e.g.* by including different kinds of particles, by allowing a reasonable variation of the parameters, introducing isospin etc., as was done in ref. [8,12,25]) for the bootstrap case).

The different behaviour of $\bar{N}$ also enters decisively in the energy dependence of the branching ratio σ_N/σ_{tot}. Both in a jet and in a fireball picture, the high-energy behaviour is essentially (cf. eq. (2.12))

$$R_N = \frac{\sigma_N(q^2)}{\sigma_{tot}(q^2)} \underset{N \text{ fixed}}{\sim} \exp\left[-\text{const}\,\bar{N}(q^2)\right],$$

which implies a power law decrease $((q^2)^{-3})$ in the jet picture, an exponential fall-off $(\exp[-6.2\sqrt{q^2}])$ in the fireball case. This striking difference is exhibited clearly also in the finite-energy calculation for $N = 4$ (Fig. 8).

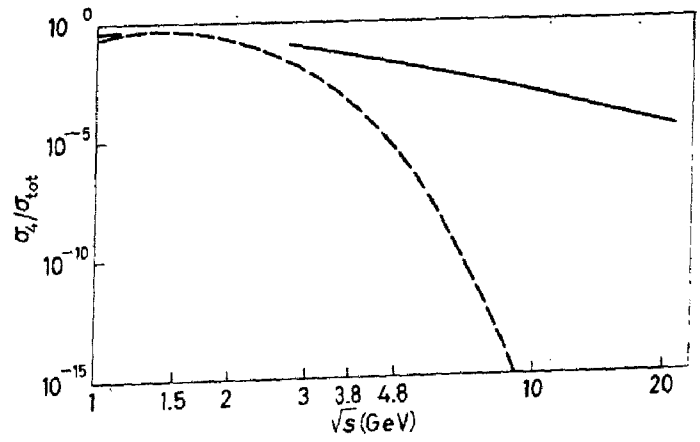

Fig. 8. – The ratio $R_4 = \sigma_4/\sigma_{tot}$; same notation as in Fig. 6.

It is not really clear, however, whether the statistical bootstrap model is ([26]) or is not ([27]) applicable to exclusive reactions.

A decisive comparison of our results to data is at present unfortunately not yet possible; measurements of $\bar{N}_{\text{total}}$, full particle identification and the corresponding spectra would be needed. Nevertheless it is instructive to compare

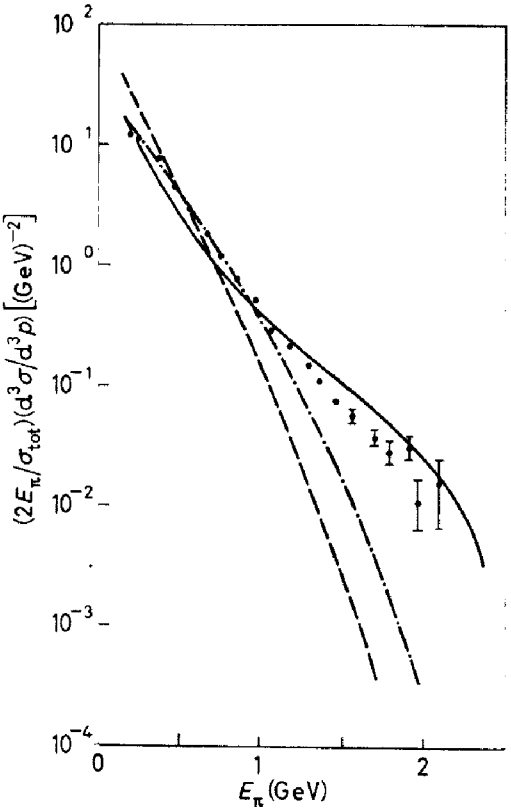

Fig. 9. – The shape of the one-particle spectrum; the curves are the same as in Fig. 5, the data for the charged-particle spectrum are from ref. ([2]) and are arbitrarily normalized.

the shape of the charged-particle spectrum with the measured energy spectrum of the observed secondaries ([2]). This is done in Fig. 9; in view of the undetermined neutral-particle yield, we have arbitrarily normalized the data. While for low secondary energies little distinction is possible, the data seem to favour the jet picture at higher E_π. On the other hand, a comparison with identified secondaries ([3]) gives good agreement with the bootstrap picture using $T_0 = 164$ MeV; we conclude from this that the experimental situation at present is still open.

Forthcoming data at somewhat higher energies could suffice to exclude the statistical bootstrap model with the mentioned T_0. As discussed in ref. ([5]),

([26]) H. J. MÖHRING, J. KRIPFGANZ, E. M. ILGENFRITZ and J. RANFT: Karl Marx Universität Leipzig preprint KMU/HEP/7405.
([27]) R. HAGEDORN and J. RANFT: *Suppl. Nuovo Cimento*, **6**, 169 (1968).

however, it is not possible to obtain definite conclusions about a jet picture from single-particle inclusive distributions. For this, two-particle correlations or exclusive measurements would be needed.

* * *

We thank P. LAURIKAINEN for valuable computational help in the early stages of this work and E. H. DE GROOT for discussions.

APPENDIX

Third-order asymptotic expansion of $\Omega(\hat{e}, q)$ etc.

In order to obtain the asymptotic expansion of the phase-space volume $\Omega(\hat{e}, q)$ eq. (2.2) for large q^2, we follow the method of ref. ([18]), which will first be sketched briefly.

Consider the Fourier transform

$$Z(\hat{e}, \beta) = \int \mathrm{d}^4 q \exp[i\beta q]\Omega(\hat{e}, q) = \exp[\varkappa z(\hat{e}, \beta)] - 1 - \varkappa z(\hat{e}, \beta)\,, \tag{A.1}$$

where

$$z(\hat{e}, \beta) = \int \frac{\mathrm{d}^3 p}{2p_0} \exp[i\beta p - \lambda |\boldsymbol{p} \times \hat{e}|]\,. \tag{A.2}$$

Because of Lorentz invariance $\Omega(\hat{e}, q)$ depends on the two variables $q_L \equiv \equiv (q_0^2 - (\hat{e}\cdot\boldsymbol{q})^2)^{\frac{1}{2}}$ and $q_T \equiv |\boldsymbol{q} \times \hat{e}|$; if we introduce the corresponding variables $\beta_L \equiv i\alpha_L$, $\alpha_L > 0$, and β_T, eqs. (A.1) and (A.2) can be written as

$$Z(\hat{e}, \beta) = 4\pi \int_0^\infty \mathrm{d}q_T\, q_T J_0(\beta_T q_T) \int_0^\infty \mathrm{d}q_L\, q_L K_0(\alpha_L q_L)\, \Omega(\hat{e}, q)\,, \tag{A.3}$$

and

$$z(\hat{e}, \beta) = 2\pi \int_0^\infty \mathrm{d}p\, p J_0(\beta_T p)\, K_0(\alpha_L \sqrt{p^2 + m^2}) \exp[-\lambda p]\,. \tag{A.4}$$

The inverse of the transformation eq. (A.3) is then given by

$$\Omega(\hat{e}, q) = \frac{1}{4\pi^2 i} \int_{\varepsilon - i\infty}^{\varepsilon + i\infty} \mathrm{d}\alpha_L\, \alpha_L I_0(\alpha_L q_L) \int_0^\infty \mathrm{d}\beta_T\, \beta_T J_0(\beta_T q_T)\, Z(\hat{e}, \beta)\,. \tag{A.5}$$

The asymptotic limit of $\Omega(\hat{e}, q)$ for large q_L is determined by the behaviour of the function $Z(\hat{e}, \beta)$ for small α_L: if we expand the Bessel function $K_0(z) = -\ln(\exp[\gamma]\cdot z/2) + O(z^2\cdot\ln z)$, γ being the Euler constant, the α_L-integration of eq. (A.5) can be performed:

$$\text{(A.6)}\quad \Omega(\hat{e}, q) = \frac{1}{\pi q_L^2}\int_0^\infty \mathrm{d}\beta_T \beta_T J_0(\beta_T q_T)\frac{\exp[-2g(\beta_T)]}{\Gamma^2(h(\beta_T))}\left(\frac{q_L}{2m}\right)^{2h(\beta_T)}\left(1 + O\left(q_L^{-2}\ln\frac{q_L}{2m}\right)\right),$$

with the functions

$$\text{(A.7)}\qquad h(\beta_T) = \pi\varkappa\int_0^\infty p\,\mathrm{d}p\, J_0(\beta_T p)\exp[-\lambda p] = \frac{\pi\varkappa}{\lambda^2}\left(1+\frac{\beta_T^2}{\lambda^2}\right)^{-1}$$

and

$$g(\beta_T) = \pi\varkappa\int_0^\infty \mathrm{d}p\, pJ_0(\beta_T p)\ln\left(\frac{\exp[\gamma]}{2}\sqrt{1+\frac{p^2}{m^2}}\right)\exp[-\lambda p].$$

A further analytic evaluation of eq. (A.6) in closed form is not possible; therefore one expands the integrand around $\beta_T = 0$, since for large q_L the power term in eq. (A.6) becomes strongly peaked around $\beta_T = 0$.

In the following we present the calculation of two additional terms to the asymptotic series of $\Omega(\hat{e}, q)$ with respect to large q_L as given in ref. [18]. For that purpose one has to take the following terms of the β_T-expansion of eq. (A.6):

$$\text{(A.8)}\quad \Omega(\hat{e}, q) = \frac{\lambda^2}{4\pi m^2}\left(\frac{q_L}{2m}\right)^{2\tilde{\varkappa}-2}\frac{\exp[-2\tilde{\varkappa}g_0]}{\Gamma^2(\tilde{\varkappa})}\int_0^\infty \mathrm{d}\beta_T\beta_T J_0(\beta_T\lambda q_T)\cdot$$

$$\cdot\exp\left[-3\tilde{\varkappa}\beta_T\ln\frac{q_L}{2m}\right]\left\{1+\beta_T^2 F^{(1)} + \beta_T^4\left(F^{(2)} + \frac{15}{4}\tilde{\varkappa}\ln\frac{q_L}{2m}\right) + \right.$$

$$\left. + \beta_T^6\left(F^{(1)} - \frac{7}{6}\right)\frac{15}{4}\tilde{\varkappa}\ln\frac{q_L}{2m} + \beta_T^8\frac{1}{2}\left(\frac{15}{4}\tilde{\varkappa}\right)^2\left(\ln\frac{q_L}{2m}\right)^2 + \ldots\right\}.$$

The dimensionless constant $\tilde{\varkappa} = \pi\varkappa/\lambda^2$ and the following short-hand notations are used:

$$\text{(A.9)}\quad \begin{cases} F^{(1)} = 3\tilde{\varkappa}\left(\psi(\tilde{\varkappa}) + \dfrac{g_1}{6}\right), \\ F^{(2)} = \dfrac{1}{8}\tilde{\varkappa}^2 g_1 - \dfrac{1}{32}\tilde{\varkappa}g_2 - \dfrac{9}{4}\tilde{\varkappa}^2\psi^{(1)}(\tilde{\varkappa}) + \dfrac{9}{2}\tilde{\varkappa}^2(\psi(\tilde{\varkappa}))^2 + \dfrac{3}{2}\tilde{\varkappa}\psi(\tilde{\varkappa})\left(g_1 - \dfrac{5}{2}\tilde{\varkappa}\right) \end{cases}$$

---

[18] All standard mathematical functions used here can be found in *Handbook of Mathematical Functions*, edited by M. ABRAMOWITZ and I. A. STEGUN (New York, N. Y.).

and

$$g_k = (2k+1)!\ln\frac{\exp[\gamma]}{2} + \frac{1}{2}(m\lambda)^{2k+2}\int_0^\infty t^{2k+1}\ln(1+t^2)\exp[-m\lambda t]\,dt =$$

$$= (2k+1)!\ln\frac{\exp[\gamma]}{2} - (m\lambda)^{2k+2}\left(-\frac{\partial}{\partial(m\lambda)}\right)^{2k+1}\left[\frac{\mathrm{Ci}(m\lambda)\cos(m\lambda)+\mathrm{si}(m\lambda)\sin(m\lambda)}{m\lambda}\right],$$

where ψ and $\psi^{(n)}$ are the digamma-function and its n-th derivative, respectively, and Ci and si are cosine and sine integrals ([28]).

The remaining Bessel transform can now be calculated, resulting finally in

$$\text{(A.10)}\qquad \Omega(\hat{e}, q) = \frac{\lambda^2\exp[-2\tilde{\varkappa}g_0](q_L/2m)^{2\tilde{\varkappa}-2}}{24\pi m^2\Gamma(\tilde{\varkappa})\Gamma(\tilde{\varkappa}+1)\ln(q_L/2m)}\exp\left[\frac{-\lambda^2 q_T^2}{12\tilde{\varkappa}\ln(q_L/2m)}\right]\cdot$$

$$\cdot\left[1 + a_0\left(\ln\frac{q_L^2}{4m^2}\right)^{-1} + (a_1 - a_2\lambda^2 q_T^2)\left(\ln\frac{q_L^2}{4m^2}\right)^{-2} + O\left(\left(\ln\frac{q_L^2}{4m^2}\right)^{-3}\right)\right]$$

with the coefficients

$$\text{(A.11)}\qquad \begin{cases} a_0 = \dfrac{2}{3\tilde{\varkappa}}\left(F^{(1)} + \dfrac{5}{2}\right), \\ a_1 = \dfrac{4}{9\tilde{\varkappa}^2}\left(2F^{(2)} + \dfrac{15}{2}F^{(1)} + 10\right), \\ a_2 = \dfrac{a_0}{3\tilde{\varkappa}} + \dfrac{5}{18\tilde{\varkappa}^2}. \end{cases}$$

In the c.m. system, $q = 0$, the dependence on the direction $\hat{e}$ drops out and therefore the integration with respect to $\hat{e}$ can trivially be written as

$$\text{(A.12)}\qquad \int d^2\hat{e}'\,\Omega(\hat{e}', q) = \Omega_{\text{c.m.s.}}(q^2).$$

For the values of $\varkappa$ and λ chosen in the model a slow approach of $\Omega_{\text{c.m.s.}}(q^2)$ to the leading term can be observed (*)

$$\text{(A.13)}\qquad \Omega_{\text{c.m.s.}}(q^2) \simeq 0.975\ (\text{GeV})^{-4}\frac{(q^2/4m^2)^{\tilde{\varkappa}-1}}{\ln(q^2/4m^2)}\cdot$$

$$\cdot\left\{1 + 5.02\left(\ln\frac{q^2}{4m^2}\right)^{-1} + 24.20\left(\ln\frac{q^2}{4m^2}\right)^{-2} + \ldots\right\}.$$

(*) We want to mention that eq. (A.13) leads to a higher value (by $\simeq 30\%$) for $\Omega_{\text{c.m.s.}}(q^2)$ at $\sqrt{q^2} = 20$ GeV than the Monte Carlo calculation.

The average multiplicity $\bar{N}$ and the correlation parameter f_2 can be obtained by differentiations of $\Omega_{\text{c.m.s.}}(q^2)$ with respect to $\varkappa$:

$$\text{(A.14)}\quad \bar{N} = \varkappa \frac{\partial}{\partial \varkappa} \ln \Omega_{\text{c.m.s.}}(q^2) = \tilde{\varkappa} \ln \frac{q^2}{4m^2} - 2\tilde{\varkappa}(g_0 + \psi(\tilde{\varkappa})) - 1 +$$
$$+ \left(\ln \frac{q^2}{4m^2}\right)^{-1} \left[2\tilde{\varkappa}\psi^{(1)}(\tilde{\varkappa}) - \frac{5}{3\tilde{\varkappa}}\right] + \left(\ln \frac{q^2}{4m^2}\right)^{-2} \cdot$$
$$\cdot \left[-\frac{55}{9\tilde{\varkappa}^2} - 2\tilde{\varkappa}\psi^{(2)}(\tilde{\varkappa}) + \frac{1}{9\tilde{\varkappa}}\left(\frac{g_2}{4} - 10g_1\right) + \frac{2}{3}\tilde{\varkappa}g_1\psi^{(1)}(\tilde{\varkappa}) + \right.$$
$$\left. + 4\tilde{\varkappa}\psi(\tilde{\varkappa})\psi^{(1)}(\tilde{\varkappa}) + \frac{10}{3}\psi^{(1)}(\tilde{\varkappa}) - \frac{10}{3\tilde{\varkappa}}\psi(\tilde{\varkappa})\right] + O\left(\left(\ln \frac{q^2}{4m^2}\right)^{-3}\right)$$

and

$$\text{(A.15)}\quad f_2 = \varkappa^2 \frac{\partial^2}{\partial \varkappa^2} \ln \Omega_{\text{c.m.s.}}(q^2) = 1 - 2\tilde{\varkappa}^2\psi^{(1)}(\tilde{\varkappa}) +$$
$$+ \left(\ln \frac{q^2}{4m^2}\right)^{-1} \left[2\tilde{\varkappa}^2\psi^{(2)}(\tilde{\varkappa}) + \frac{10}{3\tilde{\varkappa}}\right] + \left(\ln \frac{q^2}{4m^2}\right)^{-2} \cdot$$
$$\cdot \left[\frac{55}{3\tilde{\varkappa}^2} - 2\tilde{\varkappa}^2\psi^{(3)}(\tilde{\varkappa}) + 4\tilde{\varkappa}^2\psi(\tilde{\varkappa})\psi^{(2)}(\tilde{\varkappa}) + 4\tilde{\varkappa}^2\left(\psi^{(1)}(\tilde{\varkappa})\right)^2 + \right.$$
$$+ \frac{10}{3}\tilde{\varkappa}\psi^{(2)}(\tilde{\varkappa}) - \frac{20}{3}\psi^{(1)}(\tilde{\varkappa}) + \frac{20}{3\tilde{\varkappa}}\psi(\tilde{\varkappa}) + \frac{2}{3}\tilde{\varkappa}^2\psi^{(2)}(\tilde{\varkappa})g_1 +$$
$$\left. + \frac{2}{9\tilde{\varkappa}}\left(10g_1 - \frac{g_2}{4}\right)\right] + O\left(\left(\ln \frac{q^2}{4m^2}\right)^{-3}\right).$$

The corresponding numerical values can be found in eqs. (2.9)-(2.11).

The normalized N-particle cross-sections eq. (2.12) are obtained from $\Omega_{\text{c.m.s.}}(q^2)$ by

$$R_N(q^2) = \frac{1}{\Omega_{\text{c.m.s.}}(q^2)} \frac{\varkappa^N}{N!} \left[\left(\frac{\partial}{\partial \varkappa}\right)^N \Omega_{\text{c.m.s.}}(q^2)\Big|_{\varkappa=0}\right];$$

to leading order in q^2 one has [19]

$$\text{(A.16)}\quad R_N(q^2) = \frac{\Gamma^2(\tilde{\varkappa}+1)\tilde{\varkappa}^{N-1}}{(q^2/4m^2\tilde{g}_0^2)^{\tilde{\varkappa}}} \frac{1}{2\pi i} \oint \mathrm{d}t \frac{\exp\left[t \ln (q^2/4m^2\tilde{g}_0^2) - 2 \ln \Gamma(t+1)\right]}{t^N}$$

with $g_0 \equiv \ln \tilde{g}_0$. For $\ln (q^2/4m^2) \gg N$ the integral is dominated by a stationary point at $t \simeq N/\ln (q^2/4m^2\tilde{g}_0^2) \simeq 0$, yielding for large q^2

$$\text{(A.17)}\quad R_N(q^2) \xrightarrow[\ln (q^2/4m^2) \gg N]{} \frac{\Gamma^2(\tilde{\varkappa}+1)}{(q^2/4m^2\tilde{g}_0^2)^{\tilde{\varkappa}}} \frac{\left[2\tilde{\varkappa} \ln \left(\sqrt{q^2} \exp[\gamma]/2m\tilde{g}_0\right)\right]^{N-1}}{(N-1)!}.$$

For the study of the normalized inclusive single-particle spectrum $\tilde{F}(q^2; p)$ defined in eq. (2.3), we first observe that in the frame $\boldsymbol{q} = 0$ $\Omega(\hat{e}, q-p)$ is a

function of the longitudinal missing mass $M_L = \left((\sqrt{q^2} - p_0)^2 - (\hat{e}\cdot\boldsymbol{p})^2\right)^{\frac{1}{2}}$ and of $p_T = |\boldsymbol{p}\times\hat{e}|$. The expansion eq. (A.10) can be used for large M_L (with the substitutions $q_L \to M_L$ and $q_T \to p_T$):

For a fixed jet axis $\hat{e}$, and for $M_L \gg p_T$, the limiting form, eq. (2.14) follows immediately.

In order to obtain $(1/\sigma_{tot})(d\sigma/dx)$ eq. (2.4) one has to sum over the orientation $\hat{e}$.

Approximating M_L, given in eq. (2.13), by $M_L \simeq \sqrt{q^2(1-x)}$ and introducing the angle θ through $p_T = p\sin\theta$, and with $r = (\lambda/2)\sqrt{q^2}\sqrt{x^2 - 4m^2/q^2}$, one finds

$$
\begin{aligned}
(A.18)\qquad \frac{1}{\sigma_{tot}}\frac{d\sigma}{dx} &= 2\tilde{\varkappa}\frac{(1-x)^{\tilde{\varkappa}-1}}{(x^2-4m^2/q^2)^{\frac{1}{2}}}\frac{\ln(q^2/4m^2)}{\ln\left((q^2/4m^2)(1-x)\right)}\cdot \\
&\cdot\left[1 + a_0\left(\ln\frac{q^2}{4m^2}\right)^{-1} + a_1\left(\ln\frac{q^2}{4m^2}\right)^{-2} + \ldots\right]^{-1}\cdot \\
&\cdot r^3\int_0^{\pi/2} d\theta\,\sin\theta\,\exp\left[-r\sin\theta\right]\cdot\exp\left[-\frac{r^2\sin^2\theta}{6\tilde{\varkappa}\ln\left((q^2/4m^2)(1-x)\right)}\right]\cdot \\
&\cdot\left[1 + a_0\left(\ln\left(\frac{q^2}{4m^2}(1-x)\right)\right)^{-1} + (a_1 - a_2 r^2\sin^2\theta)\left(\ln\left(\frac{q^2}{4m^2}(1-x)\right)\right)^{-2} + \ldots\right].
\end{aligned}
$$

Expanding the second exponential function as well one arrives at integrals of the type

$$
\begin{aligned}
(A.19)\qquad F_n(r) \equiv \int_0^{\pi/2} d\theta(\sin\theta)^n\exp\left[-r\sin\theta\right] &= \left(-\frac{\partial}{\partial r}\right)^n\int_0^{\pi/2} d\theta\,\exp\left[-r\sin\theta\right] = \\
&= \frac{\pi}{2}\left(-\frac{\partial}{\partial r}\right)^n\left[I_0(r) - L_0(r)\right],
\end{aligned}
$$

where $L_0(r)$ is a Struve function [28]. One thus obtains

$$
\begin{aligned}
(A.20)\qquad \frac{1}{\sigma_{tot}}\frac{d\sigma}{dx} &= 2\tilde{\varkappa}\frac{(1-x)^{\tilde{\varkappa}-1}}{(x^2-4m^2/q^2)^{\frac{1}{2}}}\frac{\ln(q^2/4m^2)}{\ln\left((q^2/4m^2)(1-x)\right)}\cdot \\
&\cdot\left[1 + a_0\left(\ln\frac{q^2}{4m^2}\right)^{-1} + a_1\left(\ln\frac{q^2}{4m^2}\right)^{-2} + \ldots\right]^{-1}\cdot \\
&\cdot\left\{\left(1 + a_0\left(\ln\left(\frac{q^2}{4m^2}(1-x)\right)\right)^{-1} + a_1\left(\ln\left(\frac{q^2}{4m^2}(1-x)\right)\right)^{-2} + \ldots\right)r^2 F_1(r) - \right. \\
&- \left[1 + \left(2a_0 + \frac{5}{3\tilde{\varkappa}}\right)\left(\ln\left(\frac{q^2}{4m^2}(1-x)\right)\right)^{-1} + \ldots\right]\cdot \\
&\left.\cdot\frac{r^4 F_3(r)}{6\tilde{\varkappa}\ln\left((q^2/4m^2)(1-x)\right)} + \frac{r^6 F_5(r)}{72\tilde{\varkappa}^2}\left(\ln\frac{q^2}{4m^2}(1-x)\right)\right)^{-2} + \ldots\right\}.
\end{aligned}
$$

Finally, we discuss the approach to scaling of $(1/\sigma_{tot})(d\sigma/dx)$ resulting from eq. (A.20):

First of all there is a trivial violation of scaling due to threshold behaviour near $x \simeq x_{th} = 2m/\sqrt{q^2}$

$$\frac{1}{\sigma_{tot}}\frac{d\sigma}{dx} \simeq \frac{\tilde{\varkappa}}{2}\lambda^2 q^2 \sqrt{x^2 - \frac{4m^2}{q^2}}\,(1 + \ldots)\,. \tag{A.21}$$

With increasing x, yet large $M_L \simeq \sqrt{q^2(1-x)}$, eq. (A.20) can be approximated by

$$\frac{1}{\sigma_{tot}}\frac{d\sigma}{dx} \simeq 2\tilde{\varkappa}\frac{(1-x)^{\tilde{\varkappa}-1}}{x}\,\frac{\ln(q^2/4m^2)}{\ln\big((q^2/4m^2)(1-x)\big)}\cdot \tag{A.22}$$

$$\cdot\frac{1 + b_0\big(\ln\big((q^2/4m^2)(1-x)\big)\big)^{-1} + b_1\big(\ln\big((q/4m^2)(1-x)\big)\big)^{-2} + \ldots}{1 + a_0(\ln(q^2/4m^2))^{-1} + a_1(\ln(q^2/4m^2))^{-2} + \ldots}\,\big(1 + O\big((\lambda^2 x^2 q^2)^{-1}\big)\big)$$

with $b_0 = a_0 - 1/\tilde{\varkappa} = 4.68$ and $b_1 = a_1 - 2a_0/\tilde{\varkappa} = 20.76$.

Thus the approach to scaling is governed by a twofold expansion in the variables $(\lambda^2 x^2 q^2)^{-1}$ *and* $\big(\ln\big((q^2/4m^2)(1-x)\big)\big)^{-1}$, which imply late scaling for small x *and* for large x, respectively.

● RIASSUNTO (*)

Si applica all'annichilazione e^+e^- un modello a getto non correlato, con asse del getto orientato casualmente e parametri determinati dalle interazioni adroniche di alta energia. Si calcolano le caratteristiche risultanti (molteplicità, spettri, correlazioni, rapporti di diramazione) sia ad energie nel sistema del centro di massa finite ((3 ÷ 5) GeV) sia asintoticamente, per studiare l'approccio al comportamento asintotico previsto per quark, partoni e modelli analoghi. Si mostra che queste descrizioni, in cui la struttura del getto è uguale a quella delle interazioni adrone-adrone, portano per ragioni cinematiche ad una variazione di scala molto ritardata della distribuzione adronica inclusiva normalizzata. Si confrontano i nostri risultati con i modelli ad ammassi per l'annichilazione e^+e^- e con i dati.

(*) *Traduzione a cura della Redazione.*

Струйная структура и скейлинг при e^+e^- аннигиляции.

Резюме (*). — Модель некоррелированных струй, в которой оси струй ориентированы случайным образом и параметры определяются из адронных взаимодействий при высоких энергиях, применяется к e^+e^- аннигиляции. Вычисляются основные характеристики (множественности, спектры, корреляции, отношения ветвей) для конечных энергий в системе центра масс ((3 ÷ 5) ГэВ) и асимптотически, чтобы исследовать асимптотическое поведение, ожидаемое для моделей кварков, партонов и аналогичных моделей. Показывается, что такие описания, где струйная структура является такой же, как в случае адрон-адронных взаимодействий, из-за кинематических причин приводит к очень запоздалому скейлингу для нормализованного инклюзивного адронного распределения. Полученные результаты сравниваются с кластерными моделями для e^+e^- аннигиляции и с имеющимися экспериментальными данными.

(*) *Переведено редакцией.*